Please cite this paper as

Zhang X, Zhu Z, Yuan G, and Zhu S (2021) Adaptive Mode Selection Integrating Kalman Filter for Dynamic Response Reconstruction. Journal of Sound and Vibration. 515: 116497. https://doi.org/10.1016/j.jsv.2021.116497

Adaptive Mode Selection Integrating Kalman Filter for Dynamic Response Reconstruction

Xiao-hua Zhang, PhD
College of Civil Engineering,
Fuzhou University, Fuzhou, Fujian, China
Email: cexhzhang@fzu.edu.cn

Zimo Zhu, PhD Candidate
Department of Civil and Environmental Engineering
The Hong Kong Polytechnic University
Hong Kong, China
Email: z-zimo.zhu@connect.polyu.hk

Guo-Kai Yuan
China Energy Engineering Group Guangdong Electric Power Design Institute Co. Ltd.,
Guangzhou, Guangdong Province, China
Email: yuanguokai@gedi.com.cn

Songye Zhu*, PhD, Professor
Department of Civil and Environmental Engineering
The Hong Kong Polytechnic University
Hung Kong, China
Email: songye.zhu@polyu.edu.hk
*Corresponding author

Total number of pages: 31 pages, including title page, abstract, main text, and references
Total number of Figures: 15
Total number of tables: 4

Adaptive Mode Selection Integrating Kalman Filter for Structural Dynamic Response Reconstruction

Xiao-Hua Zhang[a], Zimo Zhu[b], Guo-Kai Yuan[c], and Songye Zhu[b,*]

[a] College of Civil Engineering, Fuzhou University, Fuzhou, Fujian, China

[b] Department of Civil and Environmental Engineering, The Hong Kong Polytechnic University, Hong Kong, China

[c] China Energy Engineering Group Guangdong Electric Power Design Institute Co. Ltd., Guangzhou, Guangdong Province, China

ABSTRACT:

Direct application of Kalman filter algorithm to state estimation of civil structures presents a computational challenge due to their high dimensions and complexity. Rewriting dynamic equations using modal coordinates can be an alternative solution to this problem because high modes with minimal contributions to structural responses can be truncated. Although the mode selection is important in accurately estimating the state of civil structures, studies on determining the remaining mode number are limited. Hence, the mode selection method in the Kalman filter for the optimal reconstruction of structural responses is investigated in this study. A modal signal-to-noise ratio (MSNR) is defined as the ratio of the estimated modal coordinate variance to the corresponding estimation error variance. Only modes with MSNR values higher than an analytically derived threshold are selected. A beam structure is numerically investigated to examine effects of excitation amplitude and frequency, measurement noise, and number of sensors on the adaptive mode selection for optimal response reconstruction. Experimental studies using a simply supported overhanging beam also confirm the efficacy of the proposed approach in response reconstruction using multiple types of sensors (including strain gauges, displacement sensors and accelerometers). Both the numerical and experimental results reveal that using all vibration modes or a complete numerical model with all degrees of freedom will reduce the accuracy of response reconstruction.

KEYWORDS:

Structural health monitoring, Kalman filter, adaptive mode selection, response reconstruction, numerical investigation, experimental studies

1. Introduction

Structural health monitoring (SHM) is a type of cutting-edge technology that ensures the safety of structures during their long service lives [1,2]. An in-depth understanding of the behavior of the entire structure is required to assessing structure safety conditions with an efficient SHM system. Thus, responses at all critical locations of a structure are often needed for the successful monitoring of structural health. However, the number of locations of monitored structural responses is considerably less than the total degrees-of-freedom (DOFs) of structures due to the economic cost associated with data acquisition and some additional practical restraints (e.g., inaccessibility of locations for sensor installation). Thus, response reconstruction at critical structural locations where sensors are unavailable is indispensable to achieve SHM objectives.

Many structural response reconstruction approaches based on limited measurements have been recently proposed. Kammer [3] put forward a response reconstruction technique in 1997 for locations without sensors based on measured responses at other locations by using a transformation matrix. Law et al. [4] proposed a method for structural response reconstruction in a full or substructure using generalized transmissibility concept in the frequency domain. Li et al. [5] extended this approach to wavelet domain for structural response estimation under unknown traffic-induced vibrations in 2017. In 2019, He and Zhou [6] developed a novel approach for reconstructing structural responses of critical locations using measurements from remote sensors based on empirical mode decomposition and Fourier series fitting method. Recently, Sun et al. [7] presented a structural response reconstruction method for reconstructing responses with quasi-static and dynamic components and solving the measurement deficiency problem through principal component analysis.

The Kalman filter is a commonly used tool that provides an unbiased and recursive algorithm in the time domain to estimate the unknown state vector of a linear dynamic system that optimally uses an incomplete and noisy measurement set [8,9]. Kalman filter-based methods consider uncertainties in structural systems and measurements. For example, Zhu et al. [10] presented a Kalman filter-based response reconstruction technique and they further extended the algorithm to accomplish data fusion for simultaneous acceleration, displacement,

and strain measurements through a normalization procedure [11]. Xu et al. [12] successfully applied the algorithm to the SHM of long-span suspension bridges. Kalman filter estimator also has the potential to reconstruct input excitations. Gillijns and Moor [13,14] presented the three-step unbiased minimum-variance state and input estimation technique for linear systems in 2007. This algorithm was extended by Lourens et al. [15] to reduced-order structural dynamic models. Zhang and Xu [16] proposed multitype sensor placement optimization under unknown excitation based on the three-step Kalman filter algorithm. In addition, Kalman filter estimators have also been successfully applied to fatigue predictions [17] and damage detection [18-20].

However, the direct application of the Kalman filter algorithm to civil structures with large dimensions and high complexity presents a computational challenge. Rewriting the second-order dynamic equation using modal coordinates can solve this problem by truncating high vibration modes with minimal and negligible contributions to structural responses. Determining the remaining mode number is important to estimate the structural state accurately. A common way to select modes is based on the concept of modal contribution factors developed in earthquake engineering, wherein modes are selected until the accumulated modal contribution factors are beyond a specified threshold [21]. This method has been extensively applied to civil structures, including beams [22,23], shear frames [24], bridges [25] and other building structures [26]. Xue et al. [27] proposed a mode selection method to include sufficient physical modes for the flexibility matrix identification. A predefined mode number is typically adopted in these methods, which are associated with the following limitations: (1) the contributions of individual modes to the overall dynamic behavior of a structure are variable, which depends on the structural characteristics, loading characteristics, and locations of interests; the selection of a fixed mode number cannot adapt to such variability; and (2) these methods always aim to select a sufficiently large number of modes; however, they did not realized that the inclusion of all or an excessive number of vibration modes may even reduce the accuracy of reconstructed responses due to the existence of reconstruction errors, as revealed in this study. Consequently, these aforementioned mode selection methods cannot guarantee the optimal response reconstruction. Additional emphasis should be placed on the adaptive selection of the most critical mode

shapes that can optimally reconstruct responses. In fact, the rational determination of the mode number has been overlooked in the previous response reconstruction studies.

An adaptive mode selection method in Kalman filtering for the optimized reconstruction of structural responses is presented in this study. The response reconstruction error that considers the increasing number of modes is first analyzed. A modal signal-to-noise ratio (MSNR) is then defined as the ratio of variance of the estimated modal coordinate response to variance of the corresponding reconstruction error from the Kalman filter algorithm. A threshold MSNR value is analytically derived, and modes with higher MSNR values than the threshold are subsequently retained. A cantilever beam structure is numerically investigated. The change of reconstruction errors with the increase of the selected mode number revealed for the first time that using all vibration modes (or a complete structural model) is a non-optimal solution with the presence of measurement and system noise. The effect of the excitation amplitude and frequency on mode selection is subsequently explored. The selection of the noise matrix and number of sensors are also discussed and compared with original assumptions. Experimental tests of a simply supported overhanging steel beam were conducted to verify the proposed method further. The numerical and experimental results demonstrated that the proposed method can provide effective and flexible mode selection to achieve accurate response reconstruction.

2. Theory

The mode selection method aims to choose the number of vibration modes for the optimal response reconstruction. The Kalman filter algorithm is used in the reconstruction of structural responses, in which posteriori error covariance matrix is applied to calculate MSNR values of each mode. The flowchart of the proposed algorithm is illustrated in Fig. 1.

2.1 Kalman filtering algorithm

Kalman filtering is a recursive technique for obtaining an unbiased estimation of the unknown linear dynamic system state vector from noisy measurements. The algorithm uses the following discrete state-space dynamic and measurement equations [28]

$$\begin{cases} \mathbf{z}_{k+1} = \mathbf{A}\mathbf{z}_k + \mathbf{B}\mathbf{u}_k + \mathbf{w}_k \\ \mathbf{y}_k = \mathbf{C}\mathbf{z}_k + \mathbf{D}\mathbf{u}_k + \mathbf{v}_k \end{cases}, \quad (1)$$

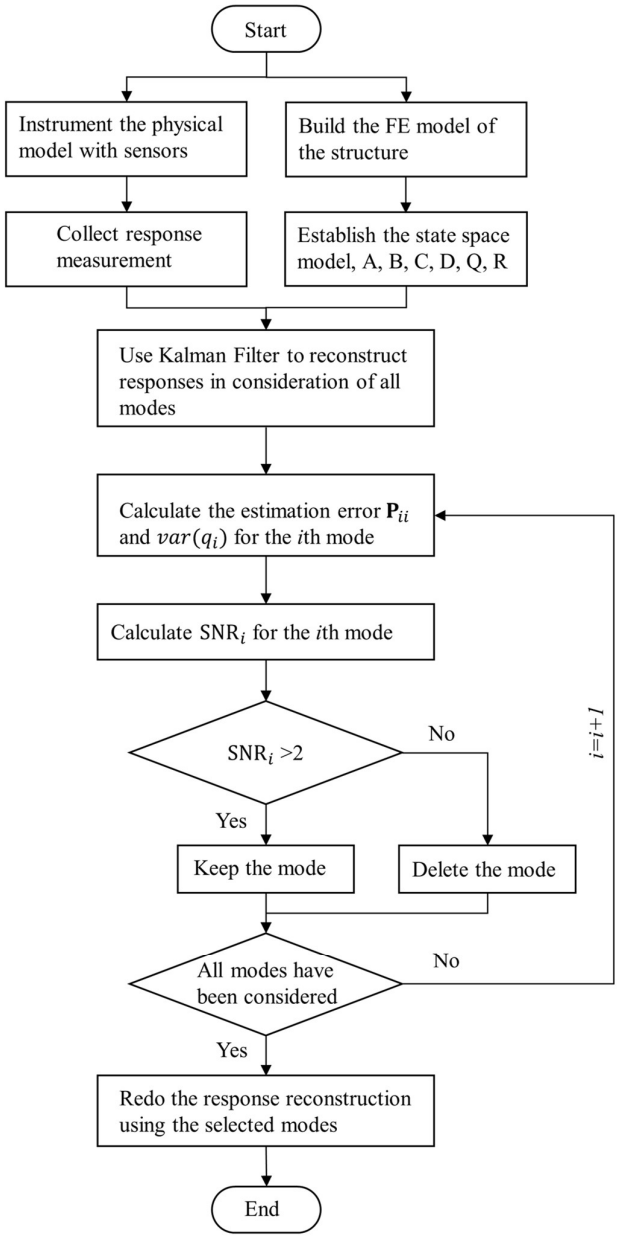

Fig. 1. Flowchart of the proposed algorithm.

where the subscript k represents the time step number; $\mathbf{z}_k$, $\mathbf{y}_k$, and $\mathbf{u}_k$ denote discrete-time state, observation, and external excitation vectors, respectively; **A** is the discrete state transmission matrix and **B** is the input matrix which relates the input excitation to state vectors; the

observation matrix **C** maps the state vector into the observed vector, while **D** is the direct transmission matrix; The process noise from modelling inaccuracies is characterized by $\mathbf{w}_k$ with covariance matrix **Q**, and measurement noise of sensors is represented by $\mathbf{v}_k$ with covariance matrix equal to **R**. It is a general practice to assume $\mathbf{w}_k$ and $\mathbf{v}_k$ are zero-mean white noise and uncorrelated to each other.

Time update and measurement update is included in the two-step Kalman filter method [9]:

$$\hat{\mathbf{z}}_{k|k-1} = \mathbf{A}\hat{\mathbf{z}}_{k-1} + \mathbf{B}\mathbf{u}_{k-1}, \tag{2}$$

$$\mathbf{P}_{k|k-1} = \mathbf{A}\mathbf{P}_{k-1}\mathbf{A}^{\mathrm{T}} + \mathbf{Q}, \tag{3}$$

$$\hat{\mathbf{z}}_k = \hat{\mathbf{z}}_{k|k-1} + \mathbf{K}_k[\mathbf{y}_k - \mathbf{C}\hat{\mathbf{z}}_{k|k-1} - \mathbf{D}\mathbf{u}_k], \tag{4}$$

$$\mathbf{P}_k = [\mathbf{I} - \mathbf{K}_k\mathbf{C}]\mathbf{P}_{k|k-1}, \tag{5}$$

$$\mathbf{K}_k = \mathbf{P}_{k|k-1}\mathbf{C}^{\mathrm{T}}[\mathbf{C}\mathbf{P}_{k|k-1}\mathbf{C}^{\mathrm{T}} + \mathbf{R}]^{-1}, \tag{6}$$

where $\mathbf{P}_k$ and $\mathbf{K}_k$ denote the covariance matrices of the estimation error in the state vector and the optimal Kalman gain, respectively, at time step k. Asymptotic values for **K** and **P** can be obtained after several iterations through Kalman filter algorithm, given any initial value of $\mathbf{P}_0$ and $\hat{\mathbf{z}}_0$.

2.2 Response Reconstruction in Modal Coordinate

Considering the computational challenge encountered by the Kalman filtering algorithm in a structure with a large number of DOFs, the structure's second-order dynamic equation can be written in the modal coordinates:

$$\ddot{\mathbf{q}} + 2\boldsymbol{\zeta}\boldsymbol{\omega}_o\dot{\mathbf{q}} + \boldsymbol{\omega}_o^2\mathbf{q} = \boldsymbol{\Phi}^{\mathrm{T}}\mathbf{B}_u\mathbf{u}, \tag{7}$$

in which the modal coordinates vector is expressed by **q**, **Φ** is the displacement mode shapes after mass normalization, $\boldsymbol{\zeta}$ denotes the modal damping coefficient matrix, $\boldsymbol{\omega}_o$ represents the modal frequency matrix, and $\mathbf{B}_u$ is the location matrix of excitations. The state-space expression of Eq. (7) can be expressed as follows:

$$\mathbf{z}_k = \begin{Bmatrix} \mathbf{q}_k \\ \dot{\mathbf{q}}_k \end{Bmatrix}, \tag{8}$$

$$\mathbf{A} = e^{\begin{bmatrix} \mathbf{0} & \mathbf{I} \\ -\boldsymbol{\omega}_o^2 & -2\boldsymbol{\zeta}\boldsymbol{\omega}_o \end{bmatrix}\Delta t}, \tag{9}$$

$$\mathbf{B} = \begin{bmatrix} \mathbf{0} & \mathbf{I} \\ -\boldsymbol{\omega}_o^2 & -2\boldsymbol{\zeta}\boldsymbol{\omega}_o \end{bmatrix}^{-1} (\mathbf{A} - \mathbf{I}) \begin{bmatrix} \mathbf{0} \\ \boldsymbol{\Phi}^{\mathrm{T}} \mathbf{B}_u \end{bmatrix}, \tag{10}$$

The observation vector $\mathbf{y}_k$ depends on the types and numbers of sensors. The utilization of multiple types of measurements can usually outperform the single type in response reconstruction. If we consider a general case with structural strains, displacements and accelerations measured, the measurement can be represented by the observation vector $\mathbf{y}_k$ and the corresponding output and direct transmission matrices can be expressed as:

$$\mathbf{y}_k = \{\boldsymbol{\varepsilon} \;\; \mathbf{d} \;\; \mathbf{a}\}^{\mathrm{T}}, \quad \mathbf{C} = \begin{bmatrix} \mathbf{E}_{sd}\boldsymbol{\Phi} & \mathbf{0} \\ \boldsymbol{\Phi} & \mathbf{0} \\ -\boldsymbol{\Phi}\boldsymbol{\omega}_0^2 & -2\boldsymbol{\Phi}\boldsymbol{\zeta}\boldsymbol{\omega}_0 \end{bmatrix}, \quad \mathbf{D} = \begin{Bmatrix} \mathbf{0} \\ \mathbf{0} \\ \boldsymbol{\Phi}\boldsymbol{\Phi}^T\mathbf{B}_u \end{Bmatrix}, \tag{11}$$

where $\boldsymbol{\varepsilon}$ is the measured strain vector, $\mathbf{d}$ is the displacement vector, $\mathbf{a}$ is the acceleration vector, and $\mathbf{E}_{sd}$ is the strain-displacement matrix relating the node displacements and element strains.

The state vector $\mathbf{z}$, including modal coordinates, is estimated using the Kalman filter algorithm on the basis of multi-type measurements. The reconstruction of displacements and strain responses at other critical locations can then be achieved through Eq. (12):

$$\mathbf{y}_k^e = \mathbf{C}^e \hat{\mathbf{z}}_k, \tag{12}$$

where the superscript "*e*" indicates the estimated or reconstructed responses, $\hat{\mathbf{z}}_k$ is the estimated state vector, $\mathbf{C}^e$ is the output matrix for the estimated strains and displacements that has a similar format to $\mathbf{C}$ but are reconstructed for different locations of interest. Matrix $\mathbf{D}^e = \{\mathbf{0} \;\; \mathbf{0}\}^{\mathrm{T}}$ is not shown in Eq. (12). The number of rows in matrices $\mathbf{C}$ and $\mathbf{C}^e$ represents the number of sensor locations and responses to be reconstructed, respectively.

If all vibration modes are considered in $\hat{\mathbf{z}}_k$, the response reconstruction performed in the modal coordinate will be the same as the conducted counterpart using mass, stiffness, and damping matrices with complete DOFs. However, considering all vibration modes in large-scale civil structures is generally unnecessary. The entire set of modes can be divided

into subsets of selected (generally lower modes with large contributions to responses) and truncated (typically higher modes with small contributions to responses) modes as follows:

$$\hat{\mathbf{z}} = \left\{ \hat{\mathbf{z}}_s \quad \hat{\mathbf{z}}_t \right\}^T = \left\{ \hat{\mathbf{q}}_s \quad \hat{\dot{\mathbf{q}}}_s \quad \hat{\mathbf{q}}_t \quad \hat{\dot{\mathbf{q}}}_t \right\}^T, \ \mathbf{C}^e = \left[\mathbf{C}_s^e \quad \mathbf{C}_t^e \right], \ \mathbf{D}^e = \left[\mathbf{D}_s^e \quad \mathbf{D}_t^e \right], \tag{13}$$

where subscripts "*s*" and "*t*" denote selected and truncated modes, respectively. Then, Eq. (12) can be rewritten as

$$\mathbf{y}^e = \mathbf{C}_s^e \hat{\mathbf{z}}_s, \tag{14}$$

Errors between reconstructed and real responses can be calculated as

$$\boldsymbol{\delta} = \mathbf{y}^e - \mathbf{y} = \mathbf{C}_s^e (\hat{\mathbf{z}}_s - \mathbf{z}_s) - \mathbf{C}_t^e \mathbf{z}_t = \boldsymbol{\delta}_n + \boldsymbol{\delta}_t, \tag{15}$$

where $\hat{\mathbf{z}}_s = \left\{ \hat{\mathbf{q}}_s \quad \hat{\dot{\mathbf{q}}}_s \right\}^T$ is the truncated state vector, $\boldsymbol{\delta}$ is the total error in reconstructed responses, $\boldsymbol{\delta}_n = \mathbf{C}_s^e (\hat{\mathbf{z}}_s - \mathbf{z}_s)$ represents estimation errors using the Kalman filter, and $\boldsymbol{\delta}_t = -\mathbf{C}_t^e \mathbf{z}_t$ represents the truncation error. The covariance matrix of reconstruction errors yields

$$\boldsymbol{\Delta} = \mathrm{cov}(\boldsymbol{\delta}) = \mathrm{cov}(\boldsymbol{\delta}_n + \boldsymbol{\delta}_t). \tag{16}$$

where $\boldsymbol{\delta}_n$ is determined by the process and measurement noise covariance matrices, and $\boldsymbol{\delta}_t$ is determined by the state vector. In the Kalman Filter, the noise covariance are commonly assumed independent with the structural responses. Therefore, it is reasonable to assume that $\boldsymbol{\delta}_n$ is also independent with $\boldsymbol{\delta}_t$, then

$$\boldsymbol{\Delta} = \mathrm{cov}(\boldsymbol{\delta}_n) + \mathrm{cov}(\boldsymbol{\delta}_t) = \Delta_n + \Delta_t, \tag{17}$$

where

$$\boldsymbol{\Delta}_n = \mathbf{C}_s^e \, \mathrm{cov}(\hat{\mathbf{z}}_s - \mathbf{z}_s) (\mathbf{C}_s^e)^{\mathrm{T}} = \mathbf{C}_s^e \mathbf{P}_s (\mathbf{C}_s^e)^{\mathrm{T}}, \tag{18}$$

$$\boldsymbol{\Delta}_t = \mathrm{cov}(\mathbf{C}_t^e \mathbf{z}_t) = \mathbf{C}_t^e \, \mathrm{cov}(\mathbf{z}_t) (\mathbf{C}_t^e)^{\mathrm{T}} \tag{19}$$

where $\mathbf{P}_s$ is the submatrix of the covariance matrix $\mathbf{P}$ of estimation errors that corresponds to selected modes. Accurate response reconstructions need to minimize $\boldsymbol{\Delta}$.

2.3 Mode Number Selection

The covariance $\boldsymbol{\Delta}$ of reconstruction errors comprise $\boldsymbol{\Delta}_n$ caused by the noise and $\boldsymbol{\Delta}_t$ induced by the truncated modes. As the number of modes in $\mathbf{P}_s$ increases, the error caused by measurement noise increases, whereas the errors caused by the truncated modes decreases. Moreover, reconstruction errors are dominated by $\boldsymbol{\Delta}_t$ when the number of selected modes is small, but dominated by $\boldsymbol{\Delta}_n$ when the number of modes increases to a certain level. This phenomenon will be illustrated in the numerical examples of this paper. Consequently, increasing the number of selected modes does not always improve the response reconstruction accuracy. Therefore, an optimal number of vibration modes must be selected to maintain the desired accuracy in the response reconstruction. This study aims at determining the required number of modes with given measurement error covariance intensity **R** and process noise covariance **Q** matrices.

Since the state vector is expressed using the modal coordinate in Eq. (8), the **P** matrix calculated in Eq. (5) represents the error covariance of the estimated modal coordinate

$$\mathbf{P} = \mathrm{E}\left[\mathbf{e}\mathbf{e}^{\mathrm{T}}\right] = \mathrm{E}\left[\left(\mathbf{z}-\hat{\mathbf{z}}\right)\left(\mathbf{z}-\hat{\mathbf{z}}\right)^{\mathrm{T}}\right] = \mathrm{E}\left[\left(\begin{Bmatrix}\mathbf{q}\\ \dot{\mathbf{q}}\end{Bmatrix} - \begin{Bmatrix}\hat{\mathbf{q}}\\ \hat{\dot{\mathbf{q}}}\end{Bmatrix}\right)\left(\begin{Bmatrix}\mathbf{q}\\ \dot{\mathbf{q}}\end{Bmatrix} - \begin{Bmatrix}\hat{\mathbf{q}}\\ \hat{\dot{\mathbf{q}}}\end{Bmatrix}\right)^{\mathrm{T}}\right], \tag{20}$$

where $\hat{\mathbf{q}}$ and $\hat{\dot{\mathbf{q}}}$ is the estimated modal displacement and velocity, respectively, both of which are composed of mode 1 to *n*; **e** is the error vector in the estimated modal coordinate. Considering the *i*th mode, as shown in Eq. (11), strains or displacements are only related to the following modal displacement q_i instead of the modal velocity $\dot{q}_i$:

$$\hat{q}_i = q_i + e_i, \tag{21}$$

where e_i is the estimation error in the *i*th modal coordinate. The variance of the estimation error e_i corresponding to the *i*th mode can be represented by the diagonal element in the covariance matrix **P**

$$p_{ii} = \mathrm{var}(e_i) = \mathrm{var}(q_i - \hat{q}_i), \quad i = 1, 2, \ldots, n, \tag{22}$$

where p_{ii} stands for the *i*th diagonal element in the **P** matrix.

According to Eq. (18) and Eq. (19), the variances of the corresponding estimation and

truncation errors of the *i*th mode can be expressed as

$$\boldsymbol{\Delta}_{n,i}=\begin{bmatrix}\mathbf{E}_{sd}\boldsymbol{\varphi}_i & \mathbf{0}\\ \boldsymbol{\varphi}_i & \mathbf{0}\end{bmatrix}\mathrm{var}(e_i)\begin{bmatrix}\mathbf{E}_{sd}\boldsymbol{\varphi}_i & \mathbf{0}\\ \boldsymbol{\varphi}_i & \mathbf{0}\end{bmatrix}^{\mathrm{T}}=\begin{bmatrix}\mathbf{E}_{sd}\boldsymbol{\varphi}_i & \mathbf{0}\\ \boldsymbol{\varphi}_i & \mathbf{0}\end{bmatrix}p_{ii}\begin{bmatrix}\boldsymbol{\varphi}_i^{\mathrm{T}}\mathbf{E}_{sd}^{\mathrm{T}} & \boldsymbol{\varphi}_i^{\mathrm{T}}\\ \mathbf{0} & \mathbf{0}\end{bmatrix}, \tag{23}$$

$$\boldsymbol{\Delta}_{t,i}=\begin{bmatrix}\mathbf{E}_{sd}\boldsymbol{\varphi}_i & \mathbf{0}\\ \boldsymbol{\varphi}_i & \mathbf{0}\end{bmatrix}\mathrm{var}(q_i)\begin{bmatrix}\mathbf{E}_{sd}\boldsymbol{\varphi}_i & \mathbf{0}\\ \boldsymbol{\varphi}_i & \mathbf{0}\end{bmatrix}^{\mathrm{T}} \tag{24}$$

where $\boldsymbol{\varphi}_i$ is the *i*th mode shape and $\mathbf{p}_{ii}$ can be calculated by Eq. (22).

The inclusion of the *i*th mode in the selected mode will introduce $\boldsymbol{\Delta}_{n,i}$ but eliminate $\boldsymbol{\Delta}_{t,i}$ in the total reconstruction error $\boldsymbol{\Delta}$; whereas the exclusion of the *i*th mode will introduce the $\boldsymbol{\Delta}_{t,i}$ but eliminate the $\boldsymbol{\Delta}_{n,i}$. It is evident that the optimal selection should be based on the relative magnitudes of $\boldsymbol{\Delta}_{n,i}$ and $\boldsymbol{\Delta}_{t,i}$ (i.e., $\mathrm{var}(e_i)$ and $\mathrm{var}(q_i)$), where $\mathrm{var}(q_i)$ represents the variance of the modal response and $\mathrm{var}(e_i)$ represents the variance of the response estimation error. By borrowing the classical concept of signal-to-noise ratio, we can define a new index as MSNR. Consequently, the *i*th mode should be included in the response reconstruction only if

$$r_i=\frac{\boldsymbol{\Delta}_{t,i}}{\boldsymbol{\Delta}_{n,i}}=\frac{\mathrm{var}(q_i)}{\mathrm{var}(e_i)}=\frac{\mathrm{var}(q_i)}{p_{ii}}>1 \tag{25}$$

Otherwise, including this mode reduces the accuracy of the response reconstruction. This also identifies the limitations of some existing response reconstruction methods that use the finite element (FE) model with all DOFs, which is essentially equivalent to the inclusion of all vibration modes in this study.

Eq. (25) can be defined as the MSNR in the *i*th mode responses. However, only the estimated modal response $\hat{q}_i$ is known in Kalman filter, while the real modal response q_i remains unknown. Thus, in practice, the estimated MSNR of the *i*th mode must be calculated as:

$$\hat{r}_i=\frac{\mathrm{var}(\hat{q}_i)}{\mathrm{var}(e_i)}=\frac{\mathrm{var}(q_i+e_i)}{\mathrm{var}(e_i)} \tag{26}$$

We can assume that q_i and e_i are two independent random variables because the

estimation error e_i comes from process and measurement noises, which are independent of structural responses. Consequently, the MSNR shown in Eq. (26) can be rewritten as:

$$\hat{r}_i = \frac{\mathrm{var}(\hat{q}_i)}{\mathrm{var}(e_i)} = \frac{\mathrm{var}(q_i) + \mathrm{var}(e_i)}{\mathrm{var}(e_i)} = \frac{\mathrm{var}(q_i)}{p_{ii}} + 1 > 2 \quad (27)$$

A large estimated MSNR $\hat{r}_i$ indicates more significant contributions of the *i*th mode to the response reconstruction, whereas a small value indicates that this mode is overwhelmed by noise. Thus, modes should be selected only if the estimated MSNR $\hat{r}_i$ is higher than this threshold. This criterion can considerably simplify the mode selection in the response reconstruction.

As illustrated by the flowchart in Fig. 1, the response reconstruction is first conducted by using all the vibration modes. Then the MSNRs are calculated for all the candidate modes individually, and those modes with the MSNRs less than the threshold are truncated. Finally, the algorithm will redo the response reconstruction using the Kalman filter and the selected modes only. The selected modes do not need to start from the first one. Neither should they be consecutive. The actual MSNRs are influenced by excitations and sensor placement, as shown in the next section. Consequently, the optimal mode selection in this approach will also adapt to the changes in these factors.

3. Numerical investigation

A two-dimensional Euler–Bernoulli cantilever beam with a length of 2.0 m and a cross section of 50.8 mm × 50.8 mm is investigated in the numerical study. The FE model comprises 21 nodes and 20 equal-length elements (Fig. 2). Ten strain measurement sensors are mounted at ten selected locations on the upper surface, as shown in Fig. 2(b). All element strains, except those at elements 19 and 20, are assumed to be reconstructed in this study, wherein strains correspond to the middle point of elements. The first ten flexural modes are considered as candidate modes, with the first four frequencies equal to 2.25, 14.11, 39.45, and 77.18 Hz.

3.1 Optimal Mode Number

Responses attained from the FE model under a vertical random excitation applied at the free end of the cantilever beam is utilized as real responses to observe the change of reconstruction errors with the increase of mode number and calculate $\boldsymbol{\Lambda}$, $\boldsymbol{\Lambda}_n$, and $\boldsymbol{\Lambda}_t$. The random excitation (Excitation 1 in Table 1) demonstrates a frequency bandwidth and maximum amplitude of 0.5–70 Hz and 50 N, respectively.

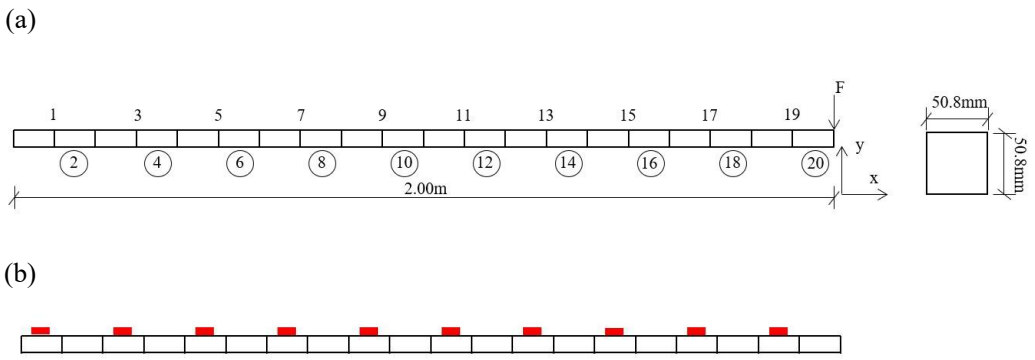

Fig. 2. Numerical investigation. (a) FE model, (b) sensor locations.

Table 1
Excitation types considered in numerical studies.

No.	Types	Frequency (Hz)
Excitation 1	Random excitation	0.5-70
Excitation 2	Non-stationary random exaction with varying amplitude	0.5-70
Excitation 3	Sine sweep excitation	0-50

Fig. 3(a) shows the variations of the reconstruction error with the increasing number of modes selected, wherein the reconstruction error is calculated as the trace of the reconstruction error matrix $\boldsymbol{\Lambda}$. The large total reconstruction error variance at the beginning is dominated by the truncated mode error Δ_t. When the mode number is equal to three, the total reconstruction error variance becomes the minimum due to small errors caused by both noise and truncated modes. When the mode number is greater than three, the total normalized reconstruction error variance Δ enlarges as the number of modes increases. The similar Δ and noise-induced error Δ_n implies a very small truncation error variance Δ_t. The minimum total normalized reconstruction error variance exhibits a minimum value of Δ

when the mode number is three. Fig. 3(b) provides a clear explanation to this selection. Only the first three modes obtain an MSNR greater than the threshold; consequently, the selection of the first three modes offers the optimal accuracy of reconstructed responses, which may be contradictory to the common practice of adopting a very detailed model in numerical simulations. If ten modes are considered in this case, then the reconstruction error will be 3.7 times the optimal value.

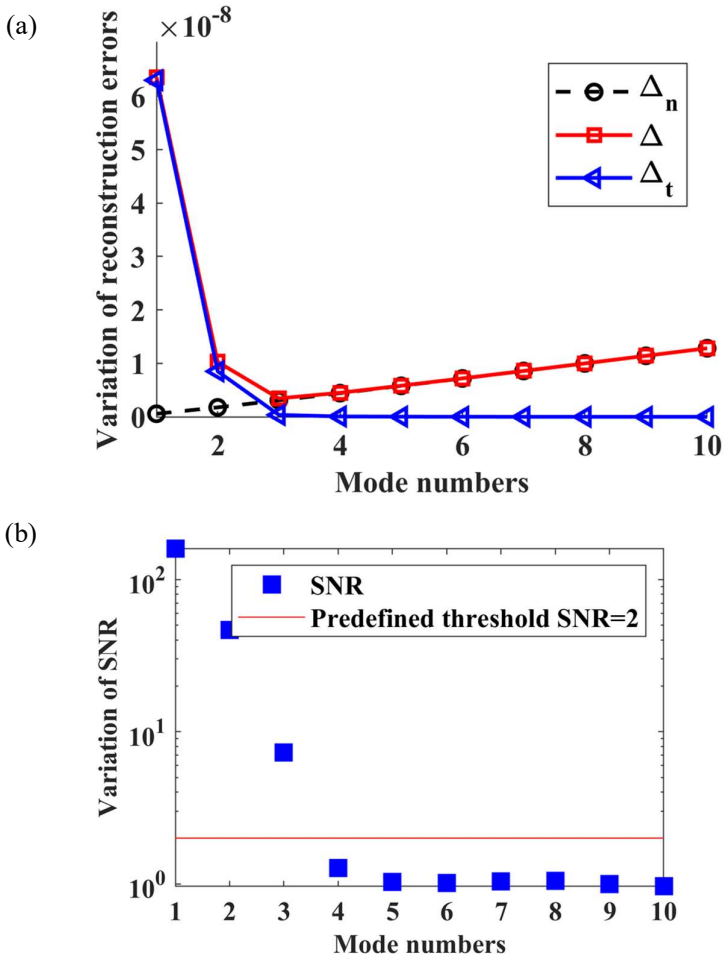

Fig. 3. Response reconstruction for the beam subjected to random excitation. (a) The variation of reconstruction errors with the increasing number of the selected modes, (b) MSNR for different vibration modes.

3.2 Effect of Excitation Amplitude

MSNRs are highly dependent on excitation amplitudes. A nonstationary random excitation (Excitation 2 in Table 1) with a frequency range of 0.5–70 Hz and varying amplitudes (i.e., maximum forces of 150, 100, 50, and 20 N in periods of 0–4, 4–8, 8–12, and 12–16 s, respectively) is applied vertically at the free end of the beam to investigate the effect of excitation amplitudes on the mode number selection. The time history of excitation is shown in Fig. 4(a). A moving window method with a window size of 1 s is applied in this study to select modes adaptively. Modes with MSNR values of $r > 2$ are selected.

Table 2 presents the results of the mode selection in each segment. Four modes with MSNRs higher than the threshold are selected in the first four seconds, when the maximum amplitude of excitation is 150 N; but reduce to three modes when the maximum amplitude of excitations are only 100 and 50 N during 4–12 seconds. Finally, two modes remain in the last four seconds when the maximum amplitude of excitation is 20 N. The decreasing amplitude of excitations clearly reduces MSNRs of all modes and consequently leads to the less selected vibration modes in the optimal response reconstruction.

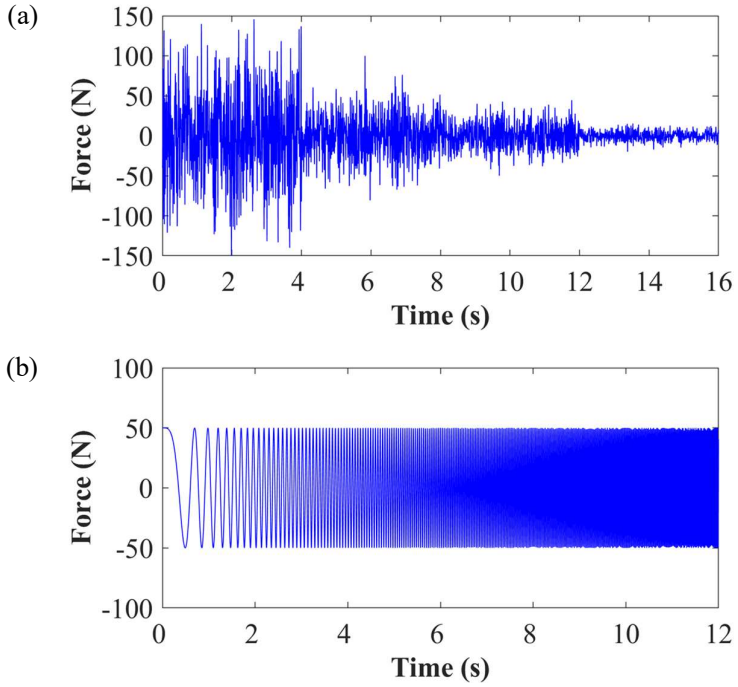

Fig. 4. Time histories of different excitations at the free end. (a) Non-stationary random excitation with varying amplitudes, (b) Sine sweeping excitations (0-50 Hz).

Table 2
Adaptive mode number selection under random excitations with varying amplitudes.

Time (s)	Excitation amplitude (N)	Selected mode number
0-1	150	1,2,3,4
1-2		1,2,3,4
2-3		1,2,3,4
3-4		1,2,3,4
4-5	100	1,2,3
5-6		1,2,3
6-7		1,2,3
7-8		1,2,3
8-9	50	1,2,3
9-10		1,2,3
10-11		1,2,3
11-12		1,2,3
12-13	20	1,2
13-14		1,2
14-15		1,2
15-16		1,2

Fig. 5 shows the comparison of variances of reconstruction errors of responses using the optimally selected modes, first five and ten flexural modes, wherein each subfigure presents errors for one excitation period (4-s period). In particular, the first ten modes were selected based on the traditional modal contribution factors. Average error variances in the reconstructed responses using ten modes are equal to 9.24×10^{-10}, 6.93×10^{-10}, 6.05×10^{-10} and, 5.46×10^{-10} for four different excitation amplitudes, and the corresponding standard deviations of errors are 3.03×10^{-5}, 2.63×10^{-5}, 2.46×10^{-10} and 2.34×10^{-10}, respectively. In order to examine the effectiveness of the proposed algorithm, the first five flexural modes are also selected to represent the scenario of randomly selecting low number of modes. The average error variances in reconstructed responses using the first five modes under four different excitation amplitudes are equal to 4.77×10^{-10}, 3.28×10^{-10}, 2.98×10^{-10} and, 2.82×10^{-10}. Average error variances of reconstructed responses using the proposed adaptive mode selection procedure reduce to 3.66×10^{-10}, 1.95×10^{-10}, 1.60×10^{-10}, and 1.21×10^{-10} under four excitation amplitudes, corresponding to standard deviations of 1.91×10^{-5}, 1.40×10^{-5}, 1.26×10^{-5}, and 1.10×10^{-5}, respectively. The error variances have 60%–80% and 20%–60% reductions when compared with results obtained by using the first 10 modes and first 5 modes,

respectively. Fig. 6 shows the time history of the strain response in element 4, including the real and reconstructed responses that use the first ten, first five flexural modes and optimally selected modes. Obviously, the use of adaptively selected modes demonstrates the smallest reconstruction errors in the responses. Reconstruction errors with selected modes reduce more significantly in the last four seconds compared with the use of all modes, because of the lower amplitude of excitation. High modes show a minimal contribution to responses but demonstrate significant discrepancies during the response reconstruction, as mentioned in the previous section. The adaptive mode selection method provides accurate response reconstruction results by selecting modes with high contribution.

3.3 Effect of Excitation Frequency

Another example that uses a sine sweeping excitation (Fig. 4(b)) is considered to investigate the effect of excitation frequency on the mode number selection, where the frequency changes from 0 Hz to 50 Hz at a rate of 4.167 Hz/s, as shown by Excitation 3 in Table 1. The frequency range covers the first three vibration modes and a slow sweeping rate is adopted to obtain steady responses under each frequency. The results of the mode selection at each segment are listed in Table 3.

Three modes have MSNRs higher than the threshold in the first nine seconds, while only two modes are selected for response reconstruction between 9 and 11 seconds. The excitation in the last second exhibits frequency content close to the beam's third and fourth natural frequencies; thus, the first, third, and fourth modes remain.

As shown in Fig. 7, compared with reconstruction errors that use the first five and ten modes, the accuracy of reconstructed responses improves significantly when the optimally selected modes are used. Average error variances of the reconstructed responses are 8.04×10^{-10}, 3.08×10^{-10}, and 2.64×10^{-10}, respectively, for the ten, five and optimal modes in the first four seconds; are 5.90×10^{-10}, 3.18×10^{-10}, and 2.77×10^{-10}, respectively, in 4–8 seconds; and are 1.16×10^{-9}, 3.40×10^{-10}, and 1.99×10^{-10} in the last four seconds. By optimally selecting the vibration modes, around 83% of errors are reduced by the proposed adaptive mode selection technique in the last four seconds compared with the reconstruction error using the first ten modes.

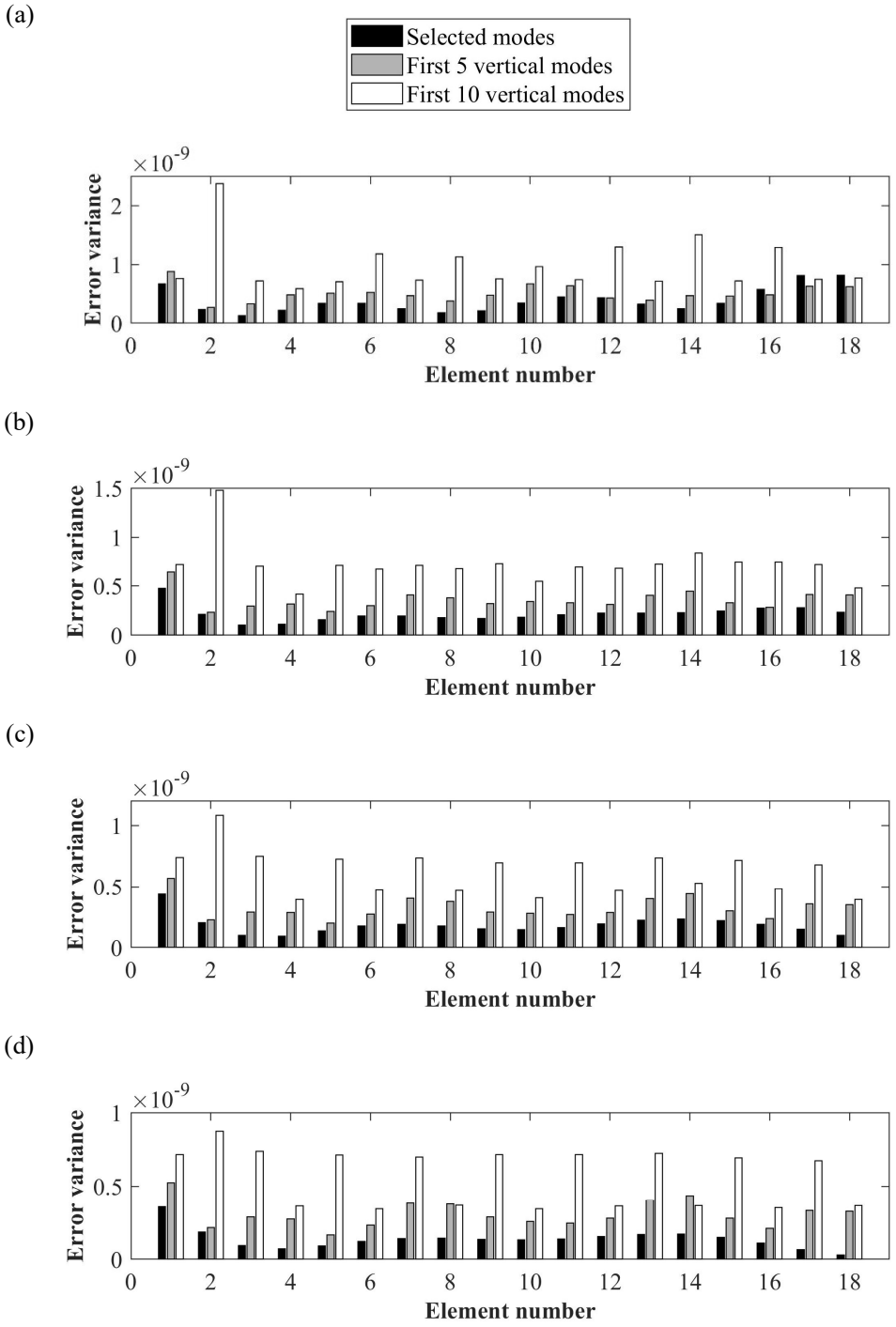

Fig. 5. Comparison of reconstruction error variances under random excitations with varying amplitudes. (a) 0-4 s, (b) 4-8 s, (c) 8-12s, (d) 12-16s.

1

(a)

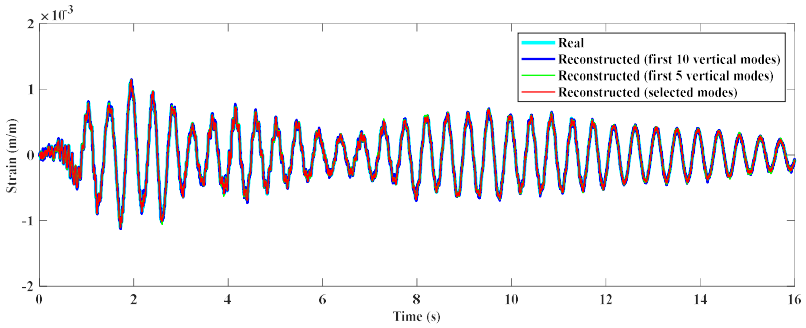

(b)

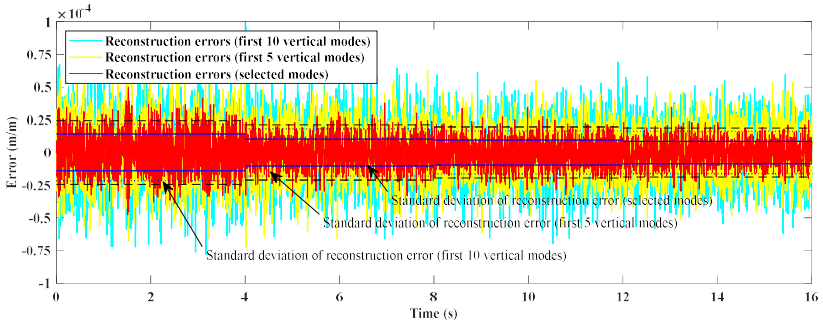

Fig. 6. Comparison of the time histories of the real and reconstructed strain responses in Element 4 under non-stationary random excitations with varying excitation amplitudes. (a) Time histories of strain responses, (b) Reconstruction errors.

Table 3

Adaptive mode number selection under sine sweeping excitation (sweep from 0 to 50 Hz).

Time (s)	Selected mode number
0-1	1,2,3
1-2	1,2,3
2-3	1,2,3
3-4	1,2,3
4-5	1,2,3
5-6	1,2,3
6-7	1,2,3
7-8	1,2,3
8-9	1,2,3
9-10	1,3
10-11	1,3
11-12	1,3,4

When compared to the reconstruction average error variances obtained by the first five

flexural modes, the error variances by the proposed algorithm have a 18%, 15% and 41% reduction in 0-4 s, 4-8 s and 8-12 s respectively, which further prove the effectiveness of the proposed adaptive mode selection algorithm. Real and reconstructed strain responses using selected and all modes are plotted in Fig. 8. The use of selected modes for response reconstruction can achieve more accurate results than using all modes. This case investigation further demonstrates the benefit of adaptive mode selection method in the response reconstruction.

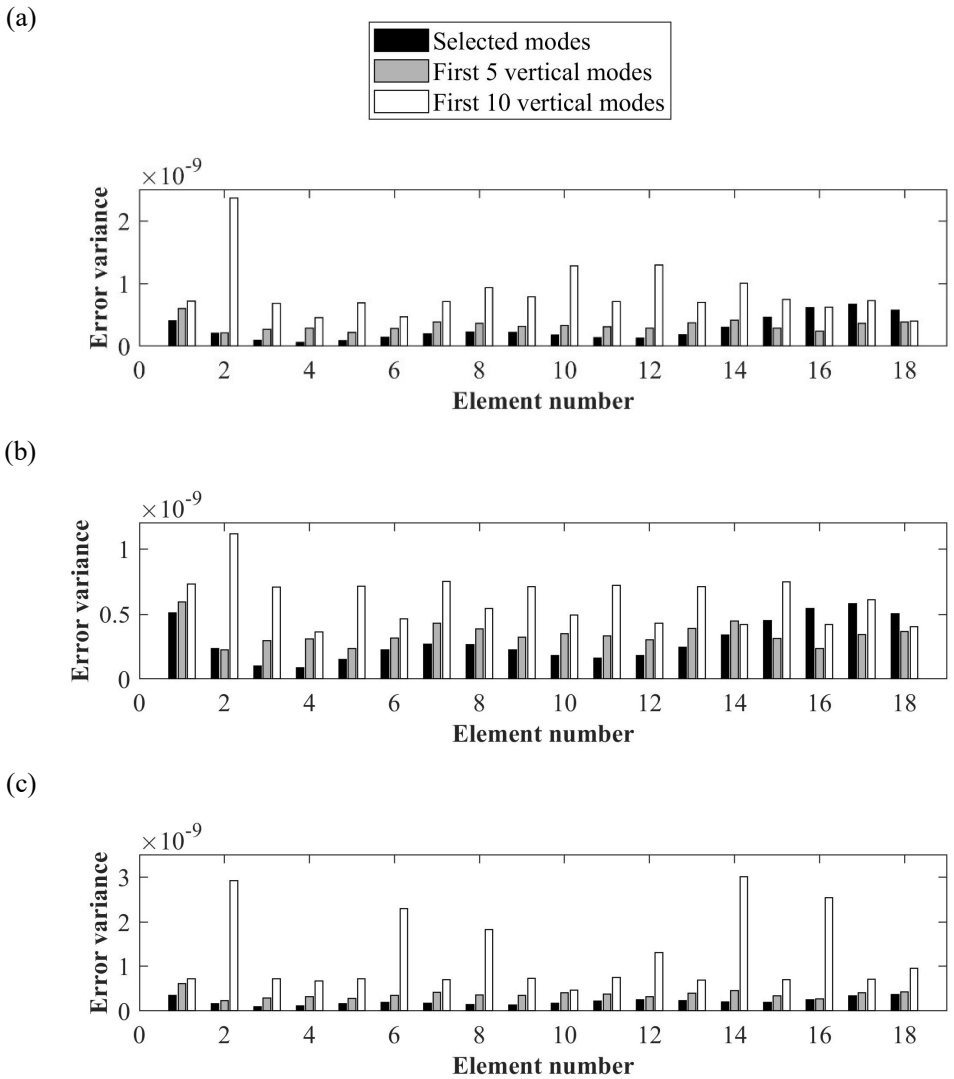

Fig. 7. Comparison of reconstruction error variances under sine sweeping excitation. (a) 0-4s, (b) 4-8s, (c) 8-12s.

3.4 Effect of Noise Level

The measurement noise is assumed as zero-mean stationary Gaussian white noise in this study. Process and measurement noise levels are assumed uncorrelated. The strain measurement noise has a constant standard deviation of 27 με, which is around 5% of the standard deviation of the largest strain responses in element 1. The measurement noise level is a major parameter that influences the response reconstruction accuracy. If the standard deviation of the strain measurement noise is set to 5.4 με (i.e., 1% of the standard deviation of the maximum strain response), which represents an extremely low noise level, then the minimum reconstruction error Δ under random excitation 1 is achieved when the first four modes are selected, as shown in Fig. 9. Compared with Fig. 3(a), the minimum reconstruction error in Fig. 9 is significantly smaller due to the reduced measurement noise. Moreover, the increase in the total reconstruction error Δ is insignificant with the increasing number of selected modes beyond four. The low measurement noise significantly reduces the noise-induced estimation error $\boldsymbol{\Delta}_n$. Consequently, the negative impact of selecting additional vibration modes is minimized and the advantage of the adaptive model selection is reduced. Thus, the measurement noise level should be carefully quantified in this method. Several Bayesian technique-based noise quantification methods have been developed recently. But they are beyond the scope of the current study and not included in this study. The system process noise covariance matrix $\mathbf{Q}$ depends on the model accuracy. If the vibration modes are identified from field measurement data, the process noise matrix $\mathbf{Q}$ shall be quantified carefully to consider the potential discrepancy between the numerical and physical models.

3.5 Effect of Number of Sensors

The number of strain gauges also directly affects the reconstruction accuracy. Ten strain gauges are assumed at selected locations in previous simulations. Fig. 10 shows the response reconstruction error when the number of sensors is reduced to only two (only available in elements 1 and 9). The optimal mode number is reduced to two, compared with three modes considered in Fig. 3(a). Meanwhile, the total reconstruction error Δ based on two sensors is larger than Δ based on ten sensors by one order of magnitude. Available sensor data affect

the measurement update step in Kalman filtering. Therefore, estimated responses rely heavily on the total number and positions of sensors. Zhang et al. [29] presented a detailed investigation on sensor placement optimization and data fusion techniques.

(a)

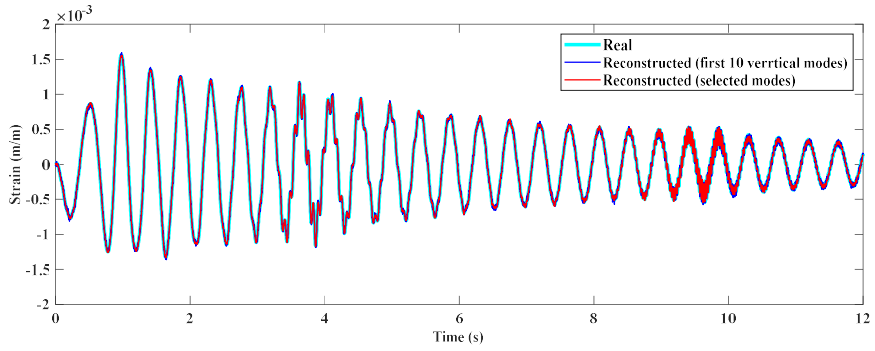

(b)

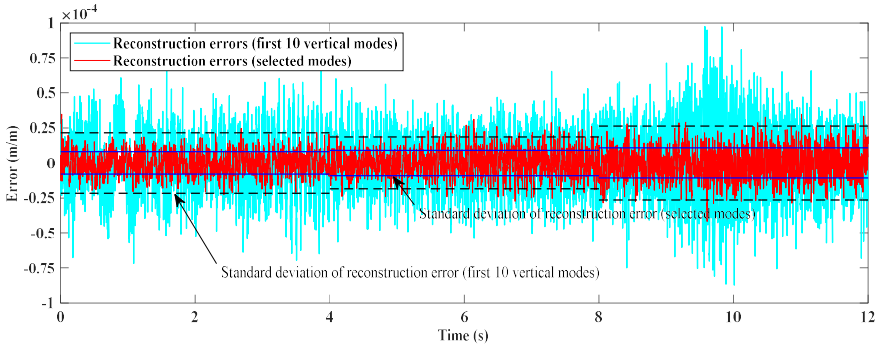

Fig. 8. Comparison of the time histories of the real and reconstructed strain responses in element 4 under sine sweeping excitation. (a) Time history, (b) Reconstruction error.

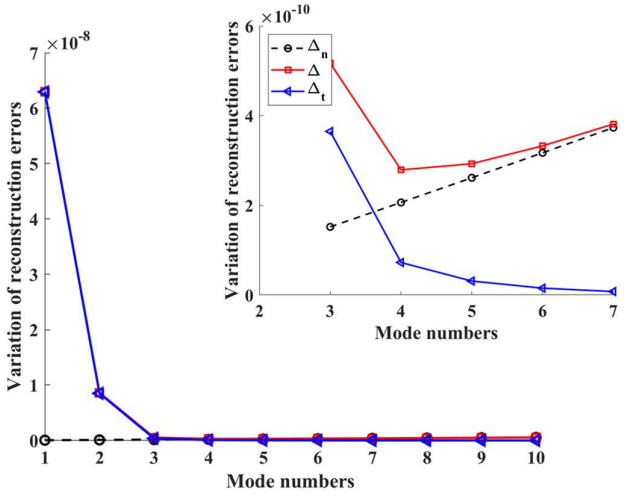

Fig. 9. Variations of reconstruction errors with increasing number of modes in consideration of a low measurement noise level.

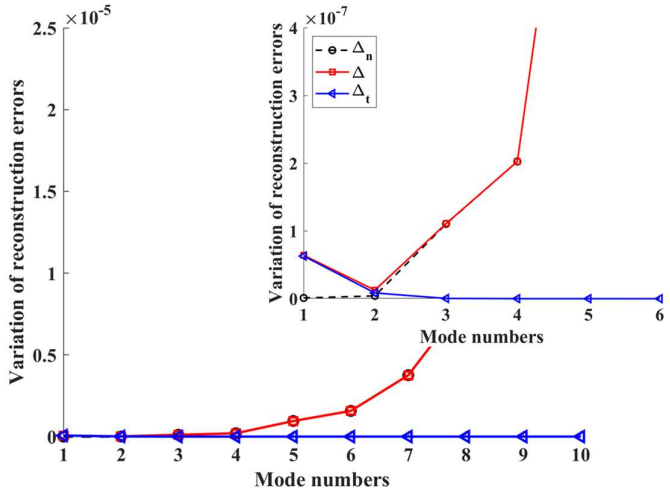

Fig. 10. Variations of reconstruction errors with increasing number of modes in consideration of only two sensors.

4. Experimental studies

A simply supported overhanging steel beam was constructed and experimentally investigated in the laboratory to authenticate the effectiveness and feasibility of the proposed adaptive mode selection method, as illustrated in Fig. 11. The total length, cross section, modulus of elasticity, and density of the beam were 4 m, 50 mm×15.65 mm (width×thickness), 2.05×10^{11} N/m^2, and 7,780 kg/m^3, respectively. The beam was then mounted on roller and hinge bearings, which were fixed on a concrete block that was attached to the ground. An updated FE model consisting of 40 elements and 41 nodes with 123 DOFs was established using commercial FE software, as shown in Fig. 12(a).

BX120-5AA resistance strain gauges, LK-503 laser displacement transducers, BK4374 and KD1008 accelerometers were employed in the experiments to measure strain, displacement and acceleration responses, respectively, as shown in Fig. 12(b). The installed sensors were divided into two sets. One set was used for the sensor measurement in the Kalman filter (Fig. 12(b)), and the other was to verify the reconstructed strain, displacement and acceleration responses at the selected locations (Fig. 12(c)). A SINOCERALC-03A force hammer was used to apply impact excitation upon the beam at the node 18 to generate the vibration. All responses were collected at a sampling rate of 500 Hz using the 32-channel data

acquisition system KYOWA EDX-100A. Figure 13 shows the measured acceleration response at node 1. The standard deviations of the measurement noises from the strain gauges, displacement transducers, and accelerometers were estimated to be 0.16 με, 0.01 mm and 0.19 m^2/s, respectively, from the measurement results. The variance of process noise is assumed as 5×10^{-9}.

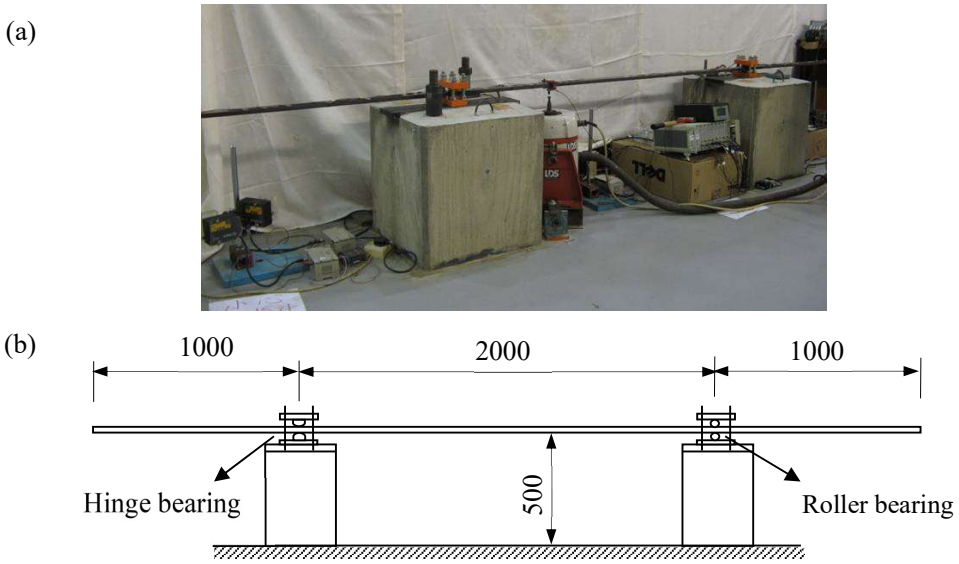

Fig. 11. Experimental studies. (a) Experimental arrangement, (b) Configuration of overhanging beam (unit: mm).

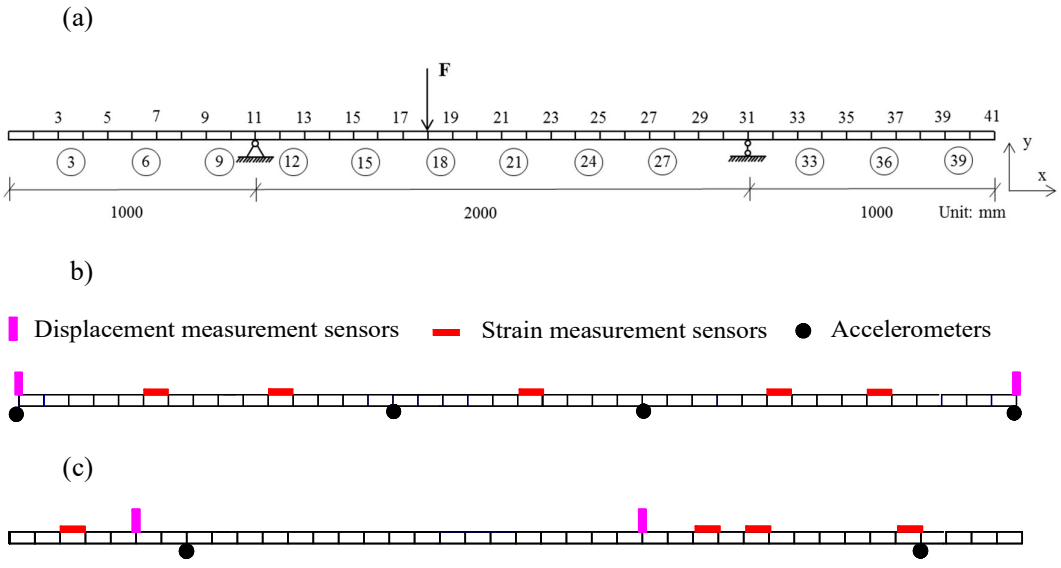

Fig. 12. FE model of the overhanging beam and sensor locations. (a) FE model of the overhanging beam (unit: mm), (b) Selected sensor locations for measurement, (c) Sensor locations for verification.

Responses at locations where sensors were unavailable were reconstructed using the measurements at the selected locations and then compared with the extra measurements to verify their accuracy. The proposed adaptive mode selection method was applied to select modes for response reconstruction. The moving window length and the threshold of the MSNR were set to 2 s and 2 respectively. Table 4 lists the modes selected for response reconstruction. The first seven modes with MSNRs higher than the threshold are selected in the first moving window; then reduce to six modes in the next moving windows; and finally decrease to five modes when the amplitude of excitation decrease in the last window.

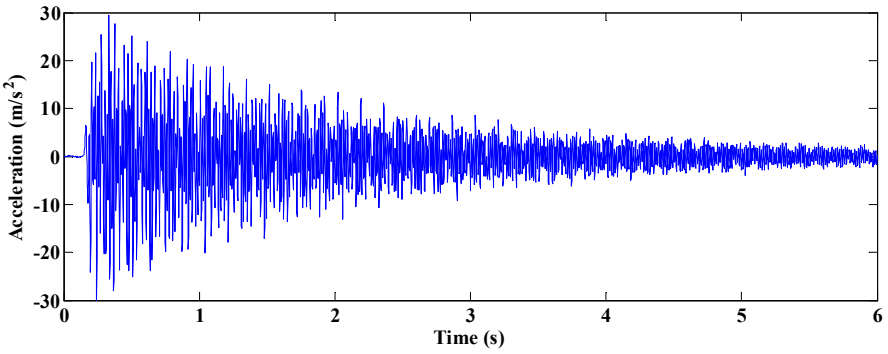

Fig. 13. Measured acceleration response at node 1 (experimental studies).

Table 4

Modes selected for response reconstruction (experimental investigation).

Time (s)	Selected mode number
0-1	1,2,3,4,5,6,7
1-2	1,2,3,4,5,6
2-3	1,2,3,5,6

Fig. 14 shows the selected reconstructed responses, including the strain time history at element 3, the displacement time history at node 6, and the acceleration time history response at node 8. The reconstructed displacement response shows similar accuracy in Fig. 14(b); however, the reconstructed strain and acceleration responses with the optimally selected modes agree with the measured response much better than those with the first 10 modes. As illustrated in Fig. 15, the use of selected modes demonstrates significantly lower reconstruction error variances than the counterparts using the first 10 modes in the strain and acceleration response reconstruction. The error variances decrease by 76% and 87%, respectively, for strain and acceleration responses compared with the original results when the

first 10 modes are used.

These experimental results further verify the effectiveness and advantage of the proposed adaptive mode selection method for response reconstruction. The application of the Kalman filter algorithm for response reconstruction in civil structures with a large number of DOFs will become more viable and accurate with a limited number of selected modes.

(a)

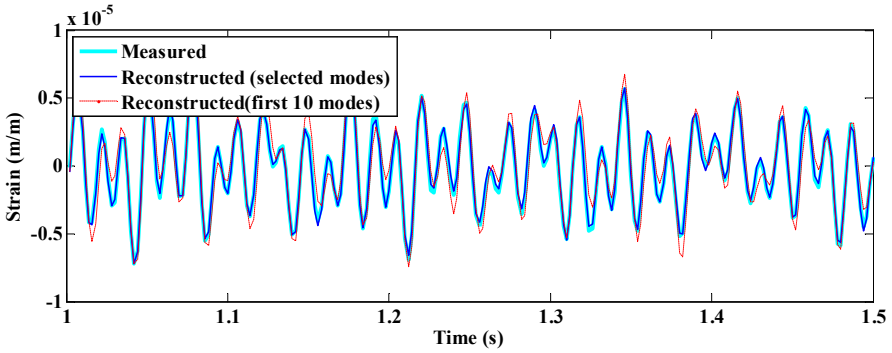

(b)

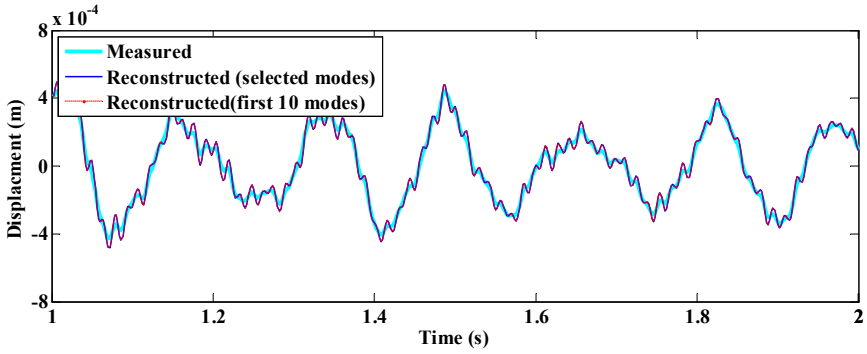

(c)

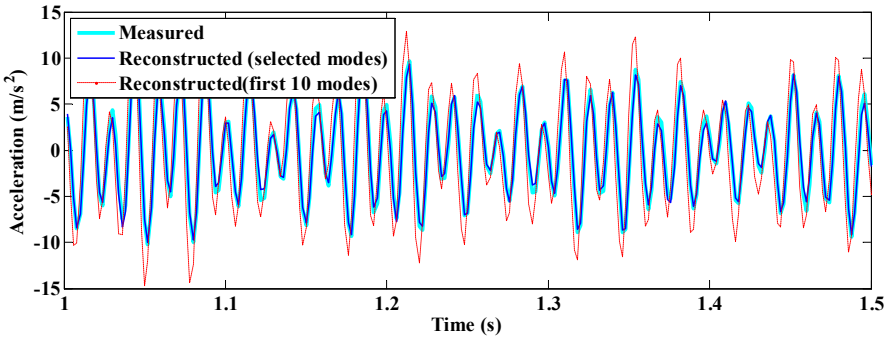

Fig. 14. Comparison of real responses, reconstructed responses using the optimally selected modes and all modes (experimental studies). (a) Strain at element 3, (b) Displacement at node 6, (c) Acceleration at node 8.

(a)

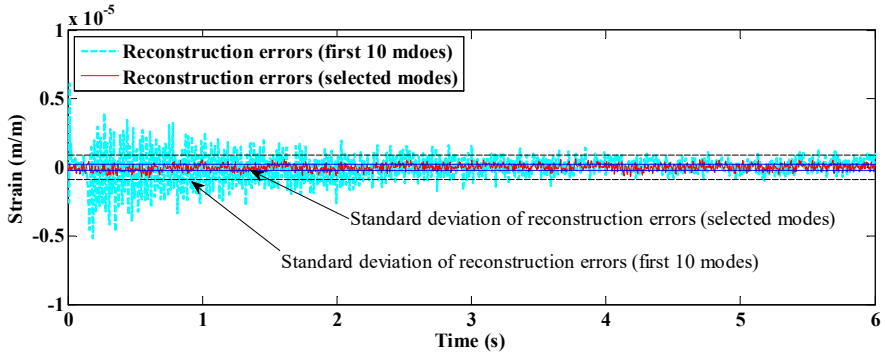

(b)

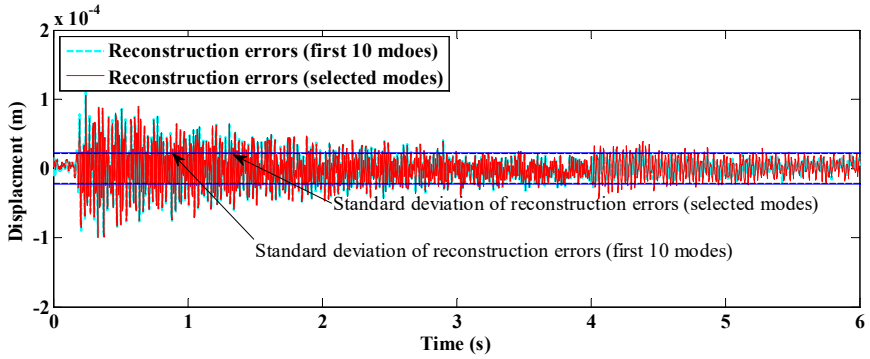

(c)

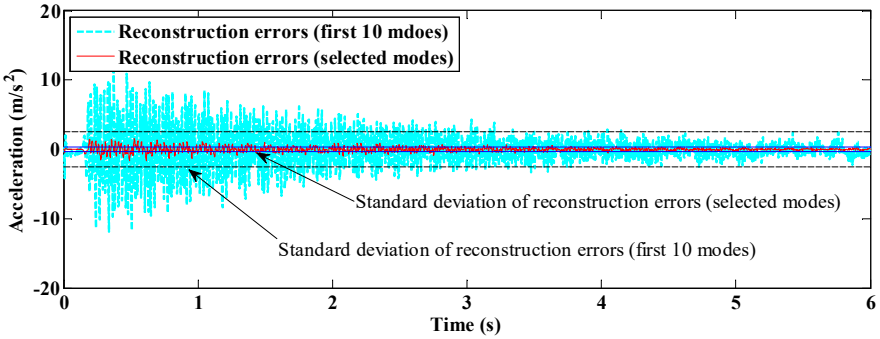

Fig. 15. Comparison of reconstruction errors (a) Strain at element 3, (b) Displacement at node 6, (c) Acceleration at node 8.

5. Conclusions

An adaptive mode selection method using the Kalman filter for response reconstruction is proposed in this study. The results revealed that reconstruction errors are due to noises and

truncated modes. Noise-induced errors increase while truncation errors decrease with the increase in the selected mode number. It is illustrated that the inclusion of all vibration modes (equivalent to a complete FE model with all DOFs) will reduce the accuracy of reconstructed responses, which has not drawn sufficient attention before. Therefore, an optimal number of modes should be selected to achieve minimum reconstruction errors. A MSNR is particularly defined to demonstrate the contribution and error levels of each mode to the response reconstruction. A threshold of 2 is analytically derived for the MSNR. Modes with MSNR > 2 should be maintained in the response reconstruction, while others should be truncated. A beam structure is numerically investigated while considering effects of excitation amplitude, excitation frequency, measurement noise level, and number of sensors. All these factors significantly influence MSNRs and thus the mode selection. Consequently, vibration modes should be adaptively selected on the basis of actual conditions to obtain the optimal response reconstruction. The results demonstrate that reconstructed responses using selected modes are more accurate than the traditional method that uses all modes. The experimental investigation using a simply supported overhanging steel beam was conducted to verify the proposed method. Data fusion for the strain, displacement, and acceleration is conducted. The consistent results further illustrate the effectiveness and accuracy of the proposed mode selection method in the response reconstruction. The results of this study can provide a theoretical basis for the application of the Kalman filter algorithm in civil structures with a large number of DOFs.

Acknowledgement

The authors wish to acknowledge the financial supports from the Special Funds for Promoting Economic Development in Guangdong Province, China (Contract of Guangdong Natural Resources Department [2019]019), the National Natural Science Foundation of China (Project No. 51608126), the National Key R&D Program of China (Project No. 2019YFB1600700), the Research Grants Council of Hong Kong (Project No. T22-502/18-R), and the GDSTC Key Technologies R&D Program (Project No. 2019B111106001).

References

[1] A. Mufti, Guidelines for structural health monitoring, Design manual 2, ISIS Canada Corp. Winnipeg, Manitoba. (2001).

[2] Y.L. Xu, Y. Xia, Structural health monitoring of long-span suspension bridges, CRC Press, 2011.

[3] D.C. Kammer, Estimation of structural response using remote sensor locations, J. Guid. Control. Dyn. 20 (1997) 501–508.

[4] S.S. Law, J. Li, Y. Ding, Structural response reconstruction with transmissibility concept in frequency domain, Mech. Syst. Signal Process. 25 (2011). https://doi.org/10.1016/j.ymssp.2010.10.001.

[5] J. Li, H. Hao, Z. Chen, Damage identification and optimal sensor placement for structures under unknown traffic-induced vibrations, J. Aerosp. Eng. 30 (2017) B4015001.

[6] J. He, Y. Zhou, A novel mode shape reconstruction method for damage diagnosis of cracked beam, Mech. Syst. Signal Process. 122 (2019) 433–447.

[7] L. Sun, Y. Li, W. Zhu, W. Zhang, Structural response reconstruction in physical coordinate from deficient measurements, Eng. Struct. 212 (2020) 110484.

[8] R.E. Kalman, A new approach to linear filtering and prediction problems, (1960).

[9] G. Welch, G. Bishop, An introduction to the Kalman filter, (1995).

[10] S. Zhu, X.H. Zhang, Y.L. Xu, S. Zhan, Multi-type sensor placement for multi-scale response reconstruction, Adv. Struct. Eng. 16 (2013) 1779–1797.

[11] X.H. Zhang, Y.L. Xu, S. Zhu, S. Zhan, Dual-type sensor placement for multi-scale response reconstruction, Mechatronics. 24 (2014) 376–384.

[12] Y.L. Xu, X.H. Zhang, S. Zhu, S. Zhan, Multi-type sensor placement and response reconstruction for structural health monitoring of long-span suspension bridges, Sci. Bull. 61 (2016) 313–329.

[13] S. Gillijns, B. De Moor, Unbiased minimum-variance input and state estimation for linear discrete-time systems, Automatica. 43 (2007) 111–116.

[14] S. Gillijns, B. De Moor, Unbiased minimum-variance input and state estimation for

linear discrete-time systems with direct feedthrough, Automatica. 43 (2007) 934–937.

[15] E. Lourens, C. Papadimitriou, S. Gillijns, E. Reynders, G. De Roeck, G. Lombaert, Joint input-response estimation for structural systems based on reduced-order models and vibration data from a limited number of sensors, Mech. Syst. Signal Process. 29 (2012) 310–327.

[16] C.D. Zhang, Y.L. Xu, Optimal multi-type sensor placement for response and excitation reconstruction, J. Sound Vib. 360 (2016) 112–128.

[17] C. Papadimitriou, C. Fritzen, P. Kraemer, E. Ntotsios, Fatigue predictions in entire body of metallic structures from a limited number of vibration sensors using Kalman filtering, Struct. Control Heal. Monit. 18 (2011) 554–573.

[18] Y. Lei, F. Chen, H. Zhou, An algorithm based on two-step Kalman filter for intelligent structural damage detection, Struct. Control Heal. Monit. 22 (2015) 694–706.

[19] C.D. Zhang, Y.L. Xu, Structural damage identification via response reconstruction under unknown excitation, Struct. Control Heal. Monit. 24 (2017) e1953.

[20] X. Xiao, Z. Sun, W. Shen, A Kalman filter algorithm for identifying track irregularities of railway bridges using vehicle dynamic responses, Mech. Syst. Signal Process. 138 (2020) 106582.

[21] A. K. Chopra, Dynamics of structures, Pearson Education India, 2017

[22] B.K. Oh, M.S. Kim, Y. Kim, T. Cho, H.S. Park, Model updating technique based on modal participation factors for beam structures, Comput-Aided Civ Inf. 30 (2015) 733-747.

[23] R. Perera, R. Huerta, J.M. Orquin, Identification of damage in RC beams using indexes based on local modal stiffness, Constr Build Mater. 22 (2008) 1656-1667.

[24] M. Palermo, S. Silverstri, G. Gasparini, T. Trombetti, Seismic modal contribution factors, Bull. Earthq. Eng. 13 (2015) 2867-2891.

[25] Z. Li, J.A. Swanson, A.J. Helmicki, V.J. Hunt, Modal contribution coefficients in bridge condition evaluation, J. Bridge Eng. 10 (2005) 169-178.

[26] N. Khodaie, Evaluation of modal contribution to the wind-induced responses of tall buildings, Asian J. Civ. Eng., 20 (2019) 837-846.

[27] M.S. Xue, T.H. Yi, C.X. Qu, H.N. Li, Structural modal flexibility identification throurh

231 a novel mode selection method. J. Eng. Mech. 147(2021)06021001.
232 [28] D. Balageas, C.P. Fritzen, A. Güemes, Structural health monitoring, John Wiley &
233 Sons, 2010.
234 [29] X.H. Zhang, S. Zhu, Y.L. X. J. Homg, Integrated optimal placement of displacement
235 transducers and strain gauges for better estimation of structural response, Int. J. Struct.
236 Stab. Dyn. 03 (2011) 581–602.